

1 **The impact of high frequency rapid viral antigen screening on COVID-19 spread and**  
2 **outcomes: a validation and modeling study**

3

4 Authors: Beatrice Nash<sup>1,2\*</sup>, Anthony Badea<sup>1,3\*</sup>, Ankita Reddy<sup>1,4\*</sup>, Miguel Bosch<sup>1,5</sup>, Nol Salcedo<sup>1</sup>,  
5 Adam R. Gomez<sup>1</sup>, Alice Versiani<sup>6</sup>, Gislaine Celestino Dutra Silva<sup>6</sup>, Thayza Maria Izabel Lopes  
6 dos Santos<sup>6</sup>, Bruno H. G. A. Milhim<sup>6</sup>, Marilia M Moraes<sup>6</sup>, Guilherme Rodrigues Fernandes  
7 Campos<sup>6</sup>, Flávia Quieroz<sup>6</sup>, Andreia Francesli Negri Reis<sup>6</sup>, Mauricio L. Nogueira<sup>6</sup>, Elena N.  
8 Naumova<sup>7</sup>, Irene Bosch<sup>1,8</sup>, Bobby Brooke Herrera<sup>1,9†</sup>

9

10 \*These authors contributed equally to this work.

11

12 Affiliations:

13 <sup>1</sup>E25Bio, Inc., Cambridge, MA, USA

14 <sup>2</sup>Department of Computer Science, Harvard University School of Engineering and Applied  
15 Sciences, Cambridge, MA, USA

16 <sup>3</sup>Department of Physics, Harvard University, Cambridge, MA, USA

17 <sup>4</sup>Perelman School of Medicine, University of Pennsylvania, Philadelphia, PA, USA

18 <sup>5</sup>InfoGeosciences LLC, Houston, TX, USA

19 <sup>6</sup>Faculdade de Medicina de São José do Rio Preto (FAMERP), São José do Rio Preto, Brazil

20 <sup>7</sup>Division of the Nutrition Epidemiology and Data Science, Friedman School of Nutrition Science  
21 and Policy, Tufts University, Boston, MA, USA

22 <sup>8</sup>Department of Medicine, Mount Sinai School of Medicine, New York, NY, USA

23 <sup>9</sup>Department of Immunology and Infectious Diseases, Harvard T.H. Chan School of Public Health,  
24 Boston, MA, USA

25

26 †Corresponding Author. BBH, email: [bbherrera@e25bio.com](mailto:bbherrera@e25bio.com)

27

28 Short Title: Modeling rapid antigen testing on COVID-19 spread

29

30

31

32

33

34

35

36

37

38

39

40

41

42

43

44

45

46 **Abstract**

47 High frequency screening of populations has been proposed as a strategy in facilitating  
48 control of the COVID-19 pandemic. Here we use computational modeling, coupled with clinical  
49 data from rapid antigen tests, to predict the impact of frequent rapid testing on COVID-19 spread  
50 and outcomes. Using patient nasal or nasopharyngeal swab specimens, we demonstrate that the  
51 sensitivity/specificity of two rapid antigen tests compared to quantitative real-time polymerase  
52 chain reaction (qRT-PCR) are 80.0%/91.1% and 84.7%/85.7%, respectively; moreover, sensitivity  
53 correlates directly with viral load. Based on COVID-19 data from three regions in the United States  
54 and São José do Rio Preto, Brazil, we show that high frequency, strategic population-wide rapid  
55 testing, even at varied accuracy levels, diminishes COVID-19 infections, hospitalizations, and  
56 deaths at a fraction of the cost of nucleic acid detection via qRT-PCR. We propose large-scale  
57 antigen-based surveillance as a viable strategy to control SARS-CoV-2 spread and to enable  
58 societal re-opening.

59

60

61

62

63

64

65

66

67

68

## 69 INTRODUCTION

70 The COVID-19 pandemic has taken an unprecedented toll on lives, wellbeing, healthcare  
71 systems, and global economies. As of 4 November 2020, there have been more than 47.6 million  
72 confirmed cases globally with more than 1 million confirmed deaths (1). However, these numbers  
73 and the current mapping of disease spread present an incomplete picture of the outbreak largely  
74 due to the lack of adequate testing, particularly as undetected infected cases are the main source  
75 of disease spread (2–7). It is estimated that the reported detection rate of actual COVID-19 cases  
76 is only 1-2% (5). As of November 2020, the United States, Brazil, and India remain the top three  
77 countries with the highest number of COVID-19 cases and deaths worldwide. As countries begin  
78 to re-open their economies, a method for accessible and frequent surveillance of COVID-19, with  
79 the necessary rapid quarantine measures, is crucial to prevent the multiple resurgences of the  
80 disease.

81 The current standard of care rightfully places a strong focus on the diagnostic limit of  
82 detection, yet frequently at the expense of both cost and turnaround time. This situation has  
83 contributed to limited population testing largely due to a dearth of diagnostic resources.  
84 Quantitative real-time polymerase chain reaction (qRT-PCR) is the gold-standard method for  
85 clinical diagnosis, with high sensitivity and specificity, but these tests are accompanied by the need  
86 for trained personnel, expensive reagents and instrumentation, and a significant amount of time to  
87 execute. Facilities offering qRT-PCR sometimes require a week or longer to complete and return  
88 the results to the patient. During this waiting period the undiagnosed individual may spread the  
89 infection and/or receive delayed medical treatment. Moreover, due to the cost and relative  
90 inaccessibility of qRT-PCR in both resource-limited and abundant settings, large-scale screening  
91 using qRT-PCR at frequent intervals remains impractical to identify infected but asymptomatic or

92 mildly symptomatic infections. Numerous studies have reported asymptomatic COVID-19 cases  
93 as well as a variation in viral load within and between individuals at different time points,  
94 suggesting the need for more frequent testing for informative surveillance.

95 Technologies alternate to qRT-PCR, such as rapid viral antigen detection, clustered  
96 regularly interspaced short palindromic repeats (CRISPR), and loop-mediated isothermal  
97 amplification (LAMP) of SARS-CoV-2 provide potential large-scale screening applications, yet  
98 their implementation is stymied by requirements for qRT-PCR-like accuracy before they can reach  
99 the market (8). In countries such as India, where the qRT-PCR resources would not be sufficient  
100 to cover monitoring of the population, the use of rapid antigen tests is well underway(9, 10). In  
101 early May 2020, the United States Food and Drug Administration (FDA) authorized the first  
102 antigen test for the laboratory detection of COVID-19, citing a need for testing beyond molecular  
103 and serological methods. Antigen testing detects the viral proteins rather than nucleic acids or  
104 human antibodies, allowing for detection of an active infection with relative ease of sample  
105 collection and assay. These rapid assays – like other commercially-available rapid antigen tests -  
106 can be mass-produced at low prices and be administered by the average person without a laboratory  
107 or instrumentation. These tests also take as little as 15 minutes to determine the result, enabling  
108 real-time surveillance and/or diagnosis. Although antigen tests usually perform with high  
109 specificities (true negative rate), their sensitivity (true positive rate) is often lower when compared  
110 to molecular assays. While qRT-PCR can reach a limit of detection as low as  $10^2$  genome copies  
111 per mL, rapid antigen testing detects viral protein that is assumed to correlate with approximately  
112  $10^5$  genome copies per mL (11).

113 We hypothesize that frequent antigen-based rapid testing even with lower sensitivities  
114 compared to qRT-PCR - along with appropriate quarantine measures - can be more effective at

115 decreasing COVID-19 spread than less frequent molecular testing of symptomatic individuals.  
116 Keeping in mind the realities of daily testing in resource-limited regions, we also hypothesize that  
117 testing frequency can be adjusted according to the prevalence of the disease; that is, an uptick in  
118 reported cases should be accompanied by more frequent testing. During the viral incubation period,  
119 high infectivity correlates with a high viral load that can be detected by either qRT-PCR or rapid  
120 antigen testing (12–16). Rapid tests thus optimize diagnosis for the most infectious individuals.  
121 Studies also point to the relatively small window of time during an individual’s incubation period  
122 in which the qRT-PCR assay is more sensitive than rapid tests (12).

123         In this study we report the clinical validation of two direct antigen rapid tests for detection  
124 of SARS-CoV-2 spike glycoprotein (S) or nucleocapsid protein (N) using retrospectively collected  
125 nasopharyngeal or nasal swab specimens. Using the clinical performance data, we develop a  
126 modeling system to evaluate the impact of frequent rapid testing on COVID-19 spread and  
127 outcomes using a variation of a SIR model, which has been previously used to model COVID-19  
128 transmission (17–23). We build on this model to incorporate quarantine states and testing protocols  
129 to examine the effects of different testing regimes. This model distinguishes between undetected  
130 and detected infections and separates severe cases, specifically, those requiring hospitalization,  
131 from those less so, which is important for disease response systems such as intensive care unit  
132 triaging. We simulate COVID-19 spread with rapid testing and model disease outcomes in three  
133 regions in the United States and São José do Rio Preto, Brazil - the site of the clinical validation  
134 study - using publicly available data. To date, COVID-19 modeling describes the course of disease  
135 spread in response to social distancing and quarantine measures, and a previous simulation study  
136 has shown that frequent testing with accuracies less than qRT-PCR, coupled with quarantine  
137 process and social distancing, are predicted to significantly decrease infections (12, 17, 23–27).

138 This is the first modeling system using publicly-available data to simulate how potential public  
139 health strategies based on testing performance, frequency, and geography impact the course of  
140 COVID-19 spread and outcomes. Our findings suggest that a rapid test, even with sensitivities  
141 lower than molecular tests, when strategically administered 2-3 times per week, will reduce  
142 COVID-19 spread, hospitalizations, and deaths at a fraction of the cost of nucleic acid testing via  
143 qRT-PCR. Modern surveillance systems should be well equipped with rapid testing tools to ensure  
144 that disease tracking and control protocols are effective and well-tailored to national, regional, and  
145 community needs.

146

## 147 **RESULTS**

### 148 **Accuracy of Direct Antigen Rapid Tests Correlate with Viral Load Levels**

149 Rapid antigen tests have recently been considered a viable source for first-line screening,  
150 although concerns about the accuracy of these tests persist. We clinically validated two different  
151 direct antigen rapid tests for the detection of either N or S from SARS-CoV-2 in retrospectively  
152 collected nasal or nasopharyngeal swab specimens. Of the total number of nasal swab specimens  
153 evaluated by qRT-PCR for amplification of SARS-CoV-2 N, S, and ORF1ab genes, 100 tested  
154 positive and 90 tested negative (Table 1, Table S1). The overall sensitivity and specificity of the  
155 rapid antigen test for detection of SARS-CoV-2 N, evaluated across the nasal swab specimens,  
156 was 80.0% and 91.1%, respectively. Of the total number of nasopharyngeal swab specimens  
157 evaluated by qRT-PCR for amplification of SARS-CoV-2 N, RNA-dependent RNA polymerase  
158 (RdRp), and envelope (E) genes, 72 tested positive and 49 tested negative (Table 2, Table S1). The  
159 overall sensitivity and specificity of the rapid antigen test for detection of SARS-CoV-2 S,  
160 evaluated across the nasopharyngeal swab specimens was 84.7% and 85.7%, respectively.

161 Altogether, our data demonstrate that the sensitivity of the rapid antigen tests are positively  
162 correlated to the viral load level (Table S1).

163 The Ct value indirectly quantifies the viral RNA copy number related to the viral load of  
164 the sample for the specific assay (28, 29). Ct values represent the number of qRT-PCR cycles at  
165 which generated fluorescence crosses a threshold during the linear amplification phase; Ct values  
166 are therefore inversely related to the viral load. The sensitivity of both rapid antigen tests increases  
167 as Ct value decreases (Table S1). Moreover, because the Ct value is a variable unit based upon  
168 qPCR protocol and instrumentation, we evaluated sensitivity against the percentile of positive  
169 cases conditioned to Ct and found similar results. The sensitivity of the rapid antigen test for  
170 detection of SARS-CoV-2 N increased from 80.0% at Ct values <40 to 95.8% at Ct values <20  
171 (Figure S1A). Similarly, the sensitivity of the rapid antigen test for detection of SARS-CoV-2 S  
172 increased from 84.7% at Ct values <35 to 100.0% at Ct values <15 (Figure S1B). Taken together,  
173 the clinical data shows that the rapid antigen test performs with increasing accuracy for individuals  
174 with a higher viral load, and potentially the most infectious (13–16).

175

## 176 **An Enhanced Epidemiological SIDHRE-Q Model**

177 We propose an enhanced epidemiological modeling system, *SIDHRE-Q*, a variant of the  
178 classical SIR model in order to expand our clinical validation study and to understand the effects  
179 of using frequent rapid tests such as the rapid antigen test on COVID-19 outbreak dynamics. The  
180 changes we make to the basic model to encompass the unique characteristics of the COVID-19  
181 pandemic are similar to those presented by Giordano et al. (16) (Figure 1, Figure S2). The  
182 differential equations governing the evolution of the *SIDHRE-Q* model and descriptions of the  
183 parameter values are provided in the material and methods section (Equation 2, Table 3).



184 An individual that begins in **S** may either transition to a Quarantine Uninfected (**Q-U**) state  
185 via a false positive result or to an Infected Undetected (**I**) state via interaction with an infected  
186 individual. Should an individual in **S** move into **Q-U**, they are quarantined for 14 days before  
187 returning to **S**, a time period chosen based on current knowledge of the infectious period of the  
188 disease. One could also conceive of an effective strategy in which individuals exit quarantine after  
189 producing a certain number of negative rapid tests in the days following their initial positive result  
190 or confirm their negative result using qRT-PCR.

191 Given that those diagnosed are predominantly quarantined, individuals in **I** interact more  
192 with the **S** population than do those in Infected Detected (**D**). Therefore, the infectious rate for **I** is  
193 assumed to be significantly larger than for **D**. Furthermore, a region's ability to control an outbreak  
194 is directly related to how quickly and effectively people in **I** test into **D**, reducing their  
195 infectiousness through quarantine. This study, in particular, highlights the critical role frequency  
196 of testing, along with strict quarantine, has in mitigating the spread of the disease and provides  
197 specific testing strategies based on rapid tests we predict to be highly effective.

198 In this model, we assume that individuals receive a positive diagnosis before developing  
199 severe symptoms and that those with symptoms severe enough to be potentially fatal will go to the  
200 hospital. If an individual develops symptoms, we assume they are tested daily until receiving a  
201 positive result; hence, before severe symptoms develop, they will be diagnosed with high  
202 probability. Those who do not develop symptoms are tested according to the frequency of tests  
203 administered to the general population. Therefore, there is no modeled connection between **I** and  
204 **H** or between **I** and **E**. Removing these assumptions would have negligible impact on the results  
205 as these flows are very small.

206           Should an individual test positive and transition to **D**, they may either develop serious  
207 symptoms requiring care or recover. Those who develop serious symptoms and transition to state  
208 **H** will then transition to either **R** or **E**. The recovered population is inevitably tested, as infected  
209 individuals may recover without being detected. Therefore, the Quarantined Recovered (**Q-R**)  
210 state is introduced with the same connections to **R** as the connections between **S** and **Q-U**. Though  
211 the reinfection rate of SARS-CoV-2 has been a point of recent debate, it is assumed that the number  
212 of re-infected individuals is small (30–34). Therefore, individuals cannot transition from **R** to **S**,  
213 hence the separately categorized quarantined populations.

214           We considered several variations and extensions of the *SIDHRE-Q* model. In simulations,  
215 we tested additional states, such as those in the *SIDARTHE* model, which include distinctions  
216 between symptomatic and asymptomatic cases for both detected and undetected populations (17).  
217 Incorporating information about the correlations between viral load and infectivity and sensitivity  
218 were also considered. Altogether, our modeling system has been well tuned to predict the impact  
219 of high frequency rapid testing on COVID-19 spread and outcomes.

220

## 221 **Frequent Rapid Testing with Actionable Quarantining Dramatically Reduces Disease** 222 **Spread**

223           In order to demonstrate how strategies could affect the disease spread in different  
224 geographies and demographics, we used surveillance data obtained from regions of varying  
225 characteristics: the state of Massachusetts (MA), New York City (NYC), Los Angeles (LA), and  
226 São José do Rio Preto (SJRP), Brazil, the site of the rapid antigen test clinical validation study.  
227 These regions are also selected in our study due to the readily available surveillance data provided  
228 by the local governments. We fit the model to the data from each region starting 1 April 2020. At

229 this time point the disease reportedly is most advanced in NYC and least advanced in SJRP, Brazil  
230 with estimated cumulative infection rates of 7.11% and 0.12%, respectively.

231 After calibrating the *SIDHRE-Q* model, the disease spread is observed with varying  
232 validated rapid antigen test performances and frequencies (Figure 2A). Sensitivity (the ratio of true  
233 positives to the total number of positives) and specificity (the ratio of true negatives to the total  
234 number of negatives) compared to gold-standard qRT-PCR were used as measures of test  
235 accuracy.

236 The rapid test frequency is varied while maintaining an accuracy of 80% sensitivity and  
237 90% specificity, comparable to our clinical data collected in SJRP, Brazil. These testing scenarios  
238 are then compared to symptomatic testing, in which individuals receive a rapid test only when  
239 presenting symptoms, via either a rapid test or qRT-PCR. Since the primary testing regiment  
240 deployed in MA, LA, NYC and SJRP, Brazil is qRT-PCR-based and focused on symptomatic  
241 individuals, the symptomatic testing protocol via qRT-PCR is directly estimated from the data to  
242 be the rate  $\nu$  (Table 3).

243 The difference between the qRT-PCR and rapid test simulations (red and orange lines,  
244 respectively) is therefore only sensitivity of testing (Figure 2A). We assumed that test outcome  
245 probability is a function only of whether an individual is infected and independent of other factors;  
246 one can consider this a lower bound on effectiveness of a strategy, as sensitivity and infectivity  
247 are often positively correlated with antigen testing.

248 To better understand the effect of rapid testing frequency and performance on healthcare  
249 capacity and mortality rates, we simulate the testing strategy with 30%-90% sensitivity each with  
250 80% or 90% specificity against the symptomatic testing strategy (Figure S3).

251 As per our hypothesis, frequency and symptom-based testing dramatically reduced  
252 infections, simultaneous hospitalizations, and total deaths when compared to the purely symptom-  
253 based testing regiments, and infections, hospitalization, and death were reduced as frequency  
254 increased. Although testing every day was clearly most effective, even testing every fourteen days  
255 with an imperfect test gave an improvement over symptomatic testing with qRT-PCR. While the  
256 strategy works best when implemented at the very beginning of an outbreak, as demonstrated by  
257 the results in SJRP, Brazil, it also works to curb an outbreak that is already large, as demonstrated  
258 by the results in NYC. The difference between frequencies is more noticeable when the testing  
259 strategy is applied to the outbreak in NYC, leading us to hypothesize that smaller outbreaks require  
260 a lower testing frequency than larger ones; note the difference between the dependence on  
261 frequency to curb a small initial outbreak in SJRP, Brazil versus a large one in NYC (Figure 2B).

262 For test performance of 80% sensitivity and 90% specificity, the percent of the population  
263 that has been infected in total from the beginning of the outbreak to mid-July drops from 18%  
264 (MA), 11% (LA), 26% (NYC), and 11% (SJRP, Brazil) to 3%, 2%, 12%, and 0.26%, respectively,  
265 using a weekly rapid testing and quarantine strategy (with regards to predictions of overall  
266 infection rates, other studies based on seroprevalence and epidemiological predictions have  
267 reached similar conclusions (35, 36)). If testing is increased to once every three days, these  
268 numbers drop further to 1.6% (MA), 1.4% (LA), 9.4% (NYC), and 0.19% (SJRP, Brazil) (Table  
269 S2).

270 To further examine the relationship between frequency and sensitivity, we modeled the  
271 maximum number of individuals in a given state over the 105-day time period for four geographic  
272 regions (Figure 2B, Figure S4). In all four geographic regions, as frequency of testing increases,  
273 the total infections, maximum simultaneous hospitalizations, and total deaths converge to small

274 percentages regardless of the sensitivity at high frequencies. It is clear that the difference in  
275 frequency required to achieve the same result using tests of differing sensitivities is very small.  
276 For example, we predict that for the outbreak in LA, a testing strategy started on 1 April of every  
277 10 days using a test of sensitivity 90% would have resulted in 2.5% of the population having been  
278 infected, while using a test of sensitivity 30% would require a strategy of every 5 days to achieve  
279 the same number. Thus, we conclude that frequency is more important than sensitivity in curbing  
280 the spread, and a large range of sensitivities prove effective when testing sufficiently often (Figure  
281 S4). How frequently, exactly, depends on the specific outbreak and what stage it is in, which leads  
282 us to the location-based deployment strategy discussed in a later section. Frequency of testing can  
283 be significantly reduced to effectively contain the disease once the initial outbreak has been  
284 controlled; it is clear that this takes only a matter of weeks (Figure 2A).

285         On the other hand, according to the specificity of the rapid test and the quarantine duration,  
286 larger testing frequency result in a larger percent of the population quarantined (Figure 2A).  
287 Assuming a 90% rapid test specificity and 14-day quarantine duration, for the 1-, 3- and 7-day  
288 frequencies almost 60%, 38% and 20% of the population, respectively, would be quarantined. This  
289 figure may be reduced with additional rules for exiting quarantine early, such as after  
290 complementary testing. An example of such a strategy is that individuals who test positive are  
291 required to either quarantine for two weeks or produce two consecutive negative rapid tests in the  
292 two days following their positive result. Assuming 80% sensitivity and 90% specificity, those  
293 individuals will reenter the public while still infected with probability 0.04. If uninfected, that  
294 individual will exit quarantine after two days with probability 0.81. However, a compromise  
295 between the reduction of infections and the proportion of the population in quarantine would be  
296 part of the planning for the appropriate testing protocol in each community or region.

297           Additionally, while high frequency may be necessary to contain a large outbreak initially,  
298 relatively infrequent testing, such as every one or two weeks, is sufficient to keep controlled  
299 outbreaks small, while reducing the number of quarantined individuals to less than 10% of the  
300 population using a two-week mandatory quarantine.

301  
302 **A County-Based Testing Strategy Offers a Cost-effective Approach to Large-scale COVID-**  
303 **19 Surveillance**

304           To examine the effects of resource-strategic testing schemes, we modeled the COVID-19  
305 prevalence by varying testing frequency across counties of California. For this analysis, only  
306 California was analyzed because of the accessibility of the county level data and the variability of  
307 spread dynamics of the outbreaks between counties. In this scheme, the percent of active infected  
308 detected individuals in a county determines the frequency of testing. We define thresholds for the  
309 number of active detected infections that, when hit, initiate testing protocols of different  
310 frequencies depending on the threshold hit. We first tested evenly spaced thresholds for the number  
311 of detected active infections up to 1% of the population, but later adopted thresholds that were  
312 determined according to Equation 1. In Equation 1,  $D$  = population of state  $\mathbf{D}$  at the time of testing.  
313  $T$  = number of active infections which, if reached, initiates everyday testing. The days between  
314 tests are rounded to the closest integer value.

$$\text{Days between tests} = \max(1, 2 \log_2(T/D) + 1)$$

315  
316 (1)

317 The days between tests are chosen such that the detected active infections should remain near to  
318 or below  $T$ . If the initial detected active infections are greater than  $T$ , then the testing frequency  
319 of 1 will cause infections to rapidly drop. Both the threshold at which everyday testing begins and

320 the coefficient of  $\log_2 T/D$  can be modified to produce a strategy that is more or less frequent in  
321 testing or resource effective; a range of days between tests from 14 days to 1 day are used (Figure  
322 3A). The purpose of this strategy is to tailor testing based on the specific characteristics of local  
323 outbreaks in order to mitigate the overall spread faster and more efficiently. A scan over different  
324 choices of  $T$  is shown in Figure 3B; the threshold we choose in Figure 3A is 0.05% because it is  
325 successful in curbing the outbreak within the time period we consider. While the choices work for  
326 the epidemic in California at the point we start our simulations, 10 April, they do not necessarily  
327 reflect the most resource effective choices everywhere. Our analysis could be redone to select the  
328 best fine-grained strategy in other states or metropolitan areas.

329         Using a rapid test with a sensitivity of 80% and specificity of 90%, the county-based testing  
330 with threshold 0.05% reduces the active infections from 0.94% to 0.0005%, while the uniform  
331 strategy with tests administered every 7 days results in double the number of active infections  
332 (Figure 3A). As the threshold is reduced, the total cost increases while the cumulative infections,  
333 maximum percentage hospitalized, and cumulative deaths all decrease (Figure 3B). Appropriate  
334 choice of threshold is dependent on the severity of outbreaks in a specific region and available  
335 resources, both logistically and fiscally. With regional data, such as that from California used to  
336 produce Figure 3B, this study can be reproduced to calculate an efficient testing strategy that will  
337 effectively curb outbreaks of differing severities in any geographic entity.

338         Strategy B in Figure 3 consists of qRT-PCR testing uniformly applied to the highlighted  
339 population with a frequency of once weekly. The average cost per person per day is just under \$15.  
340 Despite this frequency and the accuracy of qRT-PCR, the strategy does not succeed in curbing the  
341 spread as fast as strategy A, which uses a testing sensitivity and specificity of 80% and 90%,  
342 respectively, and testing frequency that vary between counties depending on the proportion of their

343 population that is currently infected. The total cost for strategy A is estimated at a fraction of the  
344 other at \$1.53 per person per day.

345

## 346 **DISCUSSION**

347 In this study we examine the potential effects of a novel testing strategy to limit the spread  
348 of SARS-CoV-2 utilizing rapid antigen test screening approaches. Our clinical data and *SIDHRE-*  
349 *Q* modeling system demonstrate that 1) frequent rapid testing even at a range of accuracies is  
350 effective at reducing COVID-19 spread, 2) rapid antigen tests are a viable source for this strategy  
351 and diagnose the most infectious individuals, and 3) strategic geographic-based testing can  
352 optimize disease control with the amount of available resources. The information from a diagnostic  
353 test itself is of tremendous value, as it can prompt the necessary quarantine measures to prevent  
354 spread, guide proper care and triage, and provide crucial disease-tracking information. Diagnostic  
355 testing in the United States and abroad, however, has been a significant public health hurdle. The  
356 public has witnessed and experienced symptomatic individuals being denied testing due to  
357 shortages, and few testing structures for asymptomatic or mildly symptomatic individuals – a  
358 significant source of disease spread. Though several factors contributed to the stymied early  
359 response measures, such as lockdown and quarantine protocols and adherence, severe testing  
360 bottlenecks were a significant culprit (37–39). Early control measures have been shown to decrease  
361 lives lost by several orders of magnitude (40). These challenges, though exacerbated during the  
362 early months of the pandemic, remain at the forefront of the public health crises.

363 Diagnosis of SARS-CoV-2 infection by qRT-PCR is the current standard of care, yet  
364 remains expensive and requires a laboratory and experienced personnel for sample preparations  
365 and experimentation. Significantly, the turnaround time for results can be up to 10 days (41). On  
366 an individual scale, this leaves the public in limbo, preventing people from either leaving



367 quarantine if they are negative, or delaying critical care and infecting others if they are positive.  
368 On a societal level, this current testing scheme yields incomplete surveillance data on which  
369 response efforts such as societal reopening and hospital management depend. Though qRT-PCR  
370 is considered the gold-standard diagnostic method because of its high sensitivity and specificity,  
371 the logistical hurdles render it unrealistic for large-scale screening.

372         As qRT-PCR remains impractical for this strategy, and rapid tests are facing regulatory  
373 challenges because they do not perform with qRT-PCR-like accuracy, rapid test screening is either  
374 nonexistent in several countries or symptom-based. Even under best-case assumptions, findings  
375 have shown that symptom and risk-based screening strategies miss more than half of the infected  
376 individuals (42). Some have argued that the need for widespread testing is overstated due to the  
377 variability in test sensitivity and specificity (43). Here, we present alternative large-scale  
378 diagnostic tools to qRT-PCR, and show that test performance, though valuable, is secondary to  
379 widespread test frequency, which is enabled by accessibility and turnaround time. Furthermore,  
380 test affordability is essential for the successful implementation in communities most affected by  
381 infection and will to speed up the safe opening and functioning of the viral sectors of the economy.

382         Giordano et al. has modeled the evolution of SARS-CoV-2 spread, introducing a diagnosed  
383 state to elucidate the importance of population-wide testing (17). Mina et al. has examined how  
384 various test sensitivities and frequencies affect the reproductive number (12). We build upon these  
385 findings to show how in affected United States and Brazil regions, population-wide frequent and  
386 rapid testing schemes, with sensitivities ranging from 30%-90%, can be more effective in curbing  
387 the pandemic than a PCR-based scheme. Integrating real-world surveillance and clinical data into  
388 our modeling system has allowed us to incorporate regional differences - such as variances in  
389 healthcare access, state health policy and adherence, state GDP, and environmental factors - under

390 the same model. Significantly, our findings hold true across Massachusetts, New York City, Los  
391 Angeles, and São José do Rio Preto, Brazil. We also present the economic considerations of these  
392 testing regimes, showing that widespread rapid testing is more cost efficient than less frequent  
393 qRT-PCR testing. In line with these economic considerations, our model demonstrates the  
394 effectiveness of a geographic-based frequent testing regime, in which high disease prevalence  
395 areas receive more frequent testing than low disease prevalence areas.

396         Since COVID-19 is known to affect certain demographics differently, modeling would  
397 benefit from incorporating demographic information correlated with disease progression and  
398 spread to define sub-models and sets of parameters accordingly. Age, pre-existing conditions, job  
399 types, and density of population are examples of possible categories, each of which influence the  
400 risk of contracting and/or dying from COVID-19. Further studies would benefit from incorporating  
401 these ideas to better understand the effectiveness of rapid testing on identifying potential super  
402 spreading events. Future public health prevention programs should use the proposed modeling  
403 system to develop and test scenarios for precision testing and prevention.

404         Our findings also point to low-cost tools for implementation of this testing strategy, such  
405 as a rapid antigen-based test for the detection of SARS-CoV-2 proteins. We show that the rapid  
406 antigen tests perform with a range of accuracies under which disease spread can be dramatically  
407 mitigated under our model. Notably, the sensitivity is correlated to the individual's viral load,  
408 effectively diagnosing those who are potentially the most infectious with the highest accuracy. Our  
409 findings are significant because rapid antigen tests are cheaper than qRT-PCR, can be mass  
410 produced to millions per day, present results within 15 minutes, and can be administered by a  
411 nonexpert without a lab or special equipment.

412           There are several policy implications for these findings. First, our model supports that  
413 systems of high frequency rapid testing should be implemented as a first-line screening method.  
414 This can be first enabled by a more holistic regulatory evaluation of rapid diagnostics, such that  
415 policy emphasizes accessibility and turnaround time even under a range of accuracies. One can  
416 imagine a less accurate, though rapid method of first-line screening in schools, public  
417 transportation, and airports, or even at home, and a qRT-PCR-based method for second-line  
418 screening (testing those who present severe symptoms or have been in contact with infected  
419 individuals, testing in a clinical setting, etc). Second, our cost analysis and rapid antigen test data  
420 present a viable and potentially more cost-effective method for screening. Third, our county-based  
421 testing scheme presents a possible method for wide-scale screening while optimizing resources.  
422 Future studies should investigate how this selective testing strategy can be applied to different  
423 location scales to further inform health policy. Moreover, though our models analyze regions in  
424 the United States and Brazil, similar testing strategies can be considered globally in both resource  
425 limited and abundant settings due to the higher accessibility of rapid tests compared to qRT-PCR.

426           We emphasize that integral to the effectiveness of diagnostic schemes is 1) the proper  
427 adherence to quarantine measures and 2) the combined use of a variety of diagnostic methods  
428 including nucleic acid, antigen, and antibody tests. According to these models, rapid antigen tests  
429 are an ideal tool for first-line screening. Clinical molecular tests such as qRT-PCR are vital to the  
430 diagnostic landscape, particularly to re-test suspected cases that were negative on the rapid test.  
431 Because rapid tests present a higher rate of false negatives, methods such as qRT-PCR remain  
432 integral to second-line screening. Antibody tests provide important information for immunity and  
433 vaccination purposes as well as epidemiological surveillance. This model also assumes that

434 individuals will quarantine themselves before being tested and for 14 days following a positive  
435 diagnostic result.

436         Our simulations combined with real-world data demonstrate a robust modeling system and  
437 elucidates the significance of this novel testing strategy. However, there are important limitations  
438 to be considered. Differences in disease reporting between the geographical regions and the  
439 incomplete nature of COVID-19 surveillance data, often due to the lack of testing, are not  
440 considered in the model. It is imperative that the testing results, hospitalization and death statistics,  
441 and changes in protocol are reported in real-time to scientists and policy makers so that models  
442 can be accurately tuned as the pandemic develops. The model also does not take into account  
443 infrastructural limitations such as hospital capacity. Though the rapid antigen test offers several  
444 advantages such as affordability, fast turnaround time, and ease of mass production, we are also  
445 assuming that there are systems in place to implement frequent and safe low-cost screening across  
446 different communities and settings.

447         Our model underscores the need for a point-of-care or at-home test for frequent screening,  
448 particularly as lockdown restrictions ease. Regulatory agencies such as the FDA could work  
449 towards regulating rapid tests to alternative standards other than comparison to high sensitivity  
450 molecular diagnostics, as our model shows that frequency and scale of testing may overcome lower  
451 sensitivities. Rather, we could refocus policy to implement first-line screening that optimizes  
452 accuracy with efficiency and equitability.

453

454

455

456

457 **MATERIAL AND METHODS**

458 **Development of Direct Antigen Rapid Tests for the Detection of SARS-CoV-2**

459 We developed a direct antigen rapid test for the detection of the nucleocapsid protein or  
460 spike glycoprotein from SARS-CoV-2 in nasal or nasopharyngeal swab specimens as previously  
461 described (44). Briefly, the rapid antigen tests are immunochromatographic format with a visual  
462 readout using anti-N or anti-S mouse monoclonal antibodies (E25Bio, Inc., Cambridge, MA, USA)  
463 that are either coupled to 40 nm gold nanoparticles (Abcam, Cambridge, UK) or adsorbed to  
464 nitrocellulose membranes (Sartorius, Goettingen, Germany). Each rapid antigen test has a control  
465 area adjacent to the paper absorbent pad; the control is an anti-mouse Fc domain antibody (Leinco  
466 Technologies, Fenton, MO, USA) that will capture any of the antibody-conjugated gold  
467 nanoparticles to generate a control visual signal. A visual signal at the test area reflects SARS-  
468 CoV-2 N or S that is “sandwiched” between an anti-N or anti-S antibody adsorbed to the  
469 nitrocellulose membrane and a second anti-N or anti-S antibody covalently coupled to visible gold  
470 nanoparticles.

471

472 **Validation of Direct Antigen Rapid Test for the Detection of SARS-CoV-2**

473 In a retrospective study of nasal swab specimens from human patients, we compared the  
474 accuracy of the rapid antigen test for detection of SARS-CoV-2 N to the viral loads of individuals.  
475 Nasal swab specimens (n=190) were tested following approved human subjects use protocols. The  
476 nasal swab specimens were banked frozen from suspected patients submitted to PATH for routine  
477 COVID diagnosis. Prior to using the rapid test, the nasal swab specimens were validated by qRT-  
478 PCR using the FDA EUA ThermoFisher/AppliedBiosystems TaqPATH COVID-19 Combo Kit  
479 (ThermoFisher, Waltham, MA USA). The primary study under which the samples and data were

480 collected received ethical clearance from the PATH Research Ethics Committee, protocol number  
481 00004244. The nasal swab specimens were de-identified, containing no demographic data, prior  
482 to analysis.

483 The nasal swabs were originally collected in 1 mL PBS, where 50  $\mu$ l was mixed with 50  $\mu$ l  
484 of Solution Buffer (0.9% NaCl and 0.1% Triton X-100). The 100  $\mu$ l mixture was then pipetted  
485 onto the rapid antigen test for SARS-CoV-2 nucleocapsid detection and allowed to react for 15  
486 minutes. After processing of the rapid antigen test, the visual positive or negative signal was  
487 documented.

488 Additionally, in a retrospective study of nasopharyngeal swab specimens from human  
489 patients, we compared the accuracy of the rapid antigen test to the viral load of individuals.  
490 Nasopharyngeal swab specimens (n = 121) were tested in Brazil following approved human  
491 subjects use protocols. The age of study participants ranged from 1 to 95 years with an overall  
492 median of 37 years (interquartile range, 27–51 years), and 62% were female. The demographic  
493 summary of the patients are included in Table S3. The nasopharyngeal swab specimens were  
494 banked refrigerated or frozen samples from suspected patients submitted to the lab for routine  
495 COVID diagnosis. Prior to using the rapid test, the nasopharyngeal swab samples were validated  
496 by qRT-PCR using GeneFinder<sup>TM</sup> COVID-19 Plus *RealAmp* Kit (OSANGHealthcare, Anyang-si,  
497 Gyeonggi-do, Republic of Korea I). The primary study under which the samples and data were  
498 collected received ethical clearance from the Faculdade de Medicina de São José do Rio Preto  
499 (FAMERP), protocol number 31588920.0.0000.5415. All excess samples and corresponding data  
500 were banked and de-identified prior to the analyses.

501 Nasopharyngeal swab specimens (1 mL) were concentrated using Vivaspin 500 centrifugal  
502 concentrator (Sartorius, Goettingen, Germany) at 12,000 x g for 10 minutes. The concentrated

503 nasopharyngeal swab specimen retentate was transferred to a collection tube and the rapid antigen  
504 test for SARS-CoV-2 spike detection was inserted into the tube with the retentate and allowed to  
505 react for 15 minutes. After processing of the rapid antigen test, the visual positive or negative  
506 signal was documented.

507

## 508 **Data for Modeling**

509 As of August 2020, the United States and Brazil have the highest number of confirmed  
510 COVID-19 cases and deaths worldwide, with both countries reporting their first case on 26  
511 February 202) (1). Although several affected US regions could have been modeled, we look at  
512 data from Massachusetts, New York, and Los Angeles: these regions each contained “hotspots”,  
513 or areas of surging COVID-19 cases, at different points in time during the pandemic and have  
514 publicly available government-provided surveillance data. Our model is fit using data over 105  
515 days beginning on April 1 for Figure 2 and 105 days beginning on April 10 for Figure 3 (see  
516 “Modeling Parameters” in Methods). In order to understand the various testing proposals on a  
517 global scale, we performed our clinical study in and expanded the modeling study to Brazil. The  
518 specific data we use to fit our model are cumulative confirmed cases, total deaths, and number of  
519 daily hospitalizations due to COVID-19. This surveillance data was retrieved from government-  
520 provided online databases (45–51).

521

## 522 **Modeling Parameters**

523 Equation 2 below provides the exact differential equations governing the model.

$$\begin{aligned}
d\mathbf{S} &= -\mathbf{S}(\alpha\mathbf{I} + \eta\mathbf{D} + \gamma) && + \psi\mathbf{Q}_U \\
d\mathbf{I} &= -\mathbf{I}(\varepsilon + \lambda + \nu) && + \mathbf{S}(\alpha\mathbf{I} + \eta\mathbf{D}) \\
d\mathbf{D} &= -\mathbf{D}\left(\frac{\mathbf{D} + \mathbf{I}}{\mathbf{D}}\mu + \rho\right) && + \mathbf{I}(\nu + \varepsilon) \\
d\mathbf{H} &= -\mathbf{H}(\sigma + \tau) && + \mu(\mathbf{D} + \mathbf{I}) \\
d\mathbf{E} &= && + \tau\mathbf{H} \\
d\mathbf{R} &= -\gamma\mathbf{R} && + \rho\mathbf{D} + \lambda\mathbf{I} + \sigma\mathbf{H} + \psi\mathbf{Q}_R \\
d\mathbf{Q}_U &= -\psi\mathbf{Q}_U && + \gamma\mathbf{S} \\
d\mathbf{Q}_R &= -\psi\mathbf{Q}_R && + \gamma\mathbf{R}
\end{aligned}
\tag{2}$$

524

525 In order to determine the values of the parameters defining the flows between states, we use a least  
526 squares regression performed at seven day intervals in the datasets to which we fit. This allows  
527 the model to take into account the time dependent nature of the parameters, which rely on factors  
528 such as social distancing regulations and changes in testing capacity. We also fit window sizes  
529 between 1 and 21 days and find that while the fit degrades with larger window size, the overall  
530 shape of the fits do not change. We choose seven days assuming policy changes take a week to  
531 become effective and that reasonable parameters can be expected to change within this time period.  
532 Also, the seven day window size accounts for the fact that often data is not reported as diligently  
533 over the weekend. Time series of the values of the parameters for the geographic locations  
534 discussed in this paper are included in Figure S5.

535 Given the restrictions on data available for the populations of various states, varying all of  
536 the parameters results in an over parameterized system. Therefore, a subset of the model  
537 parameters are fit while the others are either extracted from other sources; see Table 3. The fitting  
538 procedure minimizes the sum of the squared residuals of the total cases, current daily  
539 hospitalizations, cumulative deaths, and percentage of total infected individuals currently  
540 hospitalized. The first three are present in the data sets while the latter is derived from the estimates  
541 of the ratio between infected undetected to infected detected individuals from the CDC Laboratory



542 Seroprevalence Survey Data (52). While this ratio changes over time, the percentage of infected  
543 individuals developing severe symptoms should remain roughly constant throughout the course of  
544 the epidemic in the different locations studied.

545 We consider the data sets for outbreaks in MA, NYC, LA, and SJRP, Brazil (45–50). While  
546 each location has testing and fatality information dating back to January, hospitalization data was  
547 not included until late March (for NYC and SJRP) and April (for MA and LA). Hence we begin  
548 our fitting procedure and testing strategy on 1 April for each of the data sets; by this point, the  
549 outbreak is advanced in NYC, substantial in MA, non-negligible, but far from its peak, in LA, and  
550 in early stages in SJRP, Brazil. Starting simulations at various stages of the outbreak allows one  
551 to see the difference in results between when a testing strategy is administered.

552 In order to determine the effectiveness of the county-based strategy when applied to the  
553 state of California, we also fit all of the counties in California with a population greater than 1.5%  
554 of that of the entire state and with greater than zero deaths. The results do not depend on these  
555 selections, but instead suggest a practical criteria to administer limited resources. The fitting is  
556 done starting 10 April for these counties, as at this point the outbreak is sufficiently well-  
557 documented in each to successfully model. For the county-level data we compute a seven day  
558 running average of each of the data sets to which we then fit in order to smooth out fluctuations in  
559 the data, likely due to reporting, which are more significant here than in the other data sets  
560 considered, as the county populations are smaller and hence discrepancies impact the smoothness  
561 of the data more. The fits for each of the counties can be found in Figure S6.

562 As one can see from Figure 1, these data sets are particularly not smooth, which indicates  
563 inefficiencies in reporting. Additionally, it is difficult to gauge their consistency within the dates  
564 provided or to compare between locations, as reporting mechanisms changed over time within the

565 same locations. Despite this lack of consistency, our model and fitting mechanism was successful  
566 in reproducing the progress of the outbreak in each data set studied.

567 The authors confirm that the data supporting the findings of this study are available within the  
568 article and/or its supplementary materials; any other data will be made available upon request. Our  
569 code can be found on github: [https://github.com/badeaa3/COVID19\\_Rapid\\_Testing](https://github.com/badeaa3/COVID19_Rapid_Testing). The code is  
570 written using python with the packages scipy, numpy, lmfit, matplotlib and plotly (53–57).

### 571 **Supplementary Materials**

572

573 **Table S1. Data summary of direct antigen rapid test (DART) for detection of SARS-CoV-2**  
574 **nucleocapsid protein and DART for detection of SARS-CoV-2 spike glycoprotein**  
575 **performance in comparison to qRT-PCR results.**

576

577 **Table S2. Summary of results of COVID-19 outcomes in 3 US Regions and Brazil as a result**  
578 **of Frequent Rapid Testing Protocol using SIDHRE-Q Model.**

579

580 **Table S3. Demographic and clinical summary of patients evaluated by the SARS-CoV-2**  
581 **Direct Antigen Rapid Test (DART).**

582

583 **Figure S1. Performance of direct antigen rapid test (DART) for the detection of SARS-**  
584 **CoV-2 (A) nucleocapsid protein and (B) spike glycoprotein.** Shown are the percentile  
585 positive cases of the total positive population conditioned to qRT-PCR Cycle Threshold (Ct).

586 Percentile Positive ranks the samples in order of high Ct to low Ct. DART sensitivity is  
587 determined by calculating true positive agreement to qRT-PCR; the plot uses an  $ax^b+c$  fit and  
588 95% confidence intervals for the sensitivity.

589

590 **Figure S2. Graphical scheme displaying the relationships between the stages of quarantine**  
591 **and infection in *SIDHRE-Q* model: Q-U, quarantine uninfected; S, susceptible (uninfected); I,**  
592 **infected undetected (pre-testing and infected); D, infected detected (infection diagnosis through**  
593 **testing); H, hospitalized (infected with life threatening symptom progression); R, recovered**  
594 **(healed); E, extinct (dead); and Q-R, quarantine recovered (healed but in quarantine by false**  
595 **positive testing).**

596

597 **Figure S3. COVID-19 Outcomes as a result of Frequent Rapid Testing Protocol with**  
598 **variable test performances using *SIDHRE-Q* Model.** The Cumulative Detected Infected,  
599 Hospitalized, Deceased, Active Infections, Recovered, and Quarantined are modeled over 105  
600 days (top to bottom) using reported data from 4 global regions: Massachusetts, Los Angeles,  
601 New York City, and São José do Rio Preto in Brazil (left to right). The COVID-19 population  
602 spread and outcomes are modeled under a Rapid Testing Protocol with variable testing  
603 frequencies ranging from 1-21 days between tests, and variable test performances: 90%  
604 specificity with 90% sensitivity (A), 70% sensitivity (B), 50% sensitivity (C), and 30%  
605 sensitivity (D); and 80% specificity with 90% sensitivity (E), 70% sensitivity (F), 50%  
606 sensitivity (G), and 30% sensitivity (H). This protocol is compared to a symptom-based Rapid  
607 Testing protocol and a symptom-based qRT-PCR protocol.

608

609 **Figure S4. Effect of Rapid Testing Protocol under variable testing sensitivities and**  
610 **increasing frequency under the *SIDHRE-Q* Model.** The Cumulative Infections, Maximum  
611 Simultaneously Hospitalized, and Deceased populations are modeled for Massachusetts, Los  
612 Angeles, New York City, and São José do Rio Preto in Brazil. The effect of increasing frequency  
613 of testing is modeled for various testing sensitivities (30%-90%) with an 80% specificity.

614

615

616 **Figure S5. Time series of the four fitted parameters  $\alpha$ ,  $\nu$ ,  $\mu$ , and  $\tau$  (left to right) for MA, LA,**  
617 **NYC, and SJRP (top to bottom).** See Table 2 in the Methods section for an explanation of the  
618 parameters. The values are extracted every seven days from data provided by the respective  
619 regions. The parameters vary significantly over time and location. Flat points occur during the  
620 seven day windows where the parameters are held constant. The fitting procedure is also outlined  
621 in the Methods section.

622

623 **Figure S6. Time series of the three fitted pieces of data Cumulative Cases, Daily**  
624 **Hospitalized, and Cumulative Deaths (left to right) for each county receiving testing in CA;**  
625 **Ventura (2A), Stanislaus (2B), Santa Clara (2C), San Joaquin (2D), San Francisco (2E), San**  
626 **Diego (2F), San Bernardino (2G), Sacramento (2H), Orange (2I), Los Angeles (2J), Kern (2K),**  
627 **Fresno (2L), Alameda (2M).** The counties included satisfy two requirements: population greater  
628 than 1.5% of the total CA population and nonzero total number of deaths at each point in time.  
629 The fitting procedure is outlined in the Methods section.

630

631

632 **References**

633 1. Coronavirus Disease (COVID-19) Situation Reports, (available at

634 <https://www.who.int/emergencies/diseases/novel-coronavirus-2019/situation-reports>).

635 2. T. F. Menkir, T. Chin, J. A. Hay, E. Surface, P. Martinez de Salazar, C. Buckee, M. J. Mina,

636 K. Khan, A. Watts, M. Lipsitch, R. Niehus, Estimating the number of undetected COVID-19

637 cases exported internationally from all of China. *medRxiv* (2020),

638 doi:10.1101/2020.03.23.20038331.

639 3. B. Ivorra, M. R. Ferrández, M. Vela-Pérez, A. M. Ramos, Mathematical modeling of the

640 spread of the coronavirus disease 2019 (COVID-19) taking into account the undetected

641 infections. The case of China. *Commun Nonlinear Sci Numer Simul*, 105303 (2020).

642 4. M. Salathé, C. L. Althaus, R. Neher, S. Stringhini, E. Hodcroft, J. Fellay, M. Zwahlen, G.

643 Senti, M. Battegay, A. Wilder-Smith, I. Eckerle, M. Egger, N. Low, COVID-19 epidemic in

644 Switzerland: on the importance of testing, contact tracing and isolation. *Swiss Med Wkly*.

645 **150**, w20225 (2020).

646 5. H. Lau, T. Khosrawipour, P. Kocbach, H. Ichii, J. Bania, V. Khosrawipour, Evaluating the

647 massive underreporting and undertesting of COVID-19 cases in multiple global epicenters.

648 *Pulmonology* (2020), doi:10.1016/j.pulmoe.2020.05.015.

- 649 6. J. D. Silverman, N. Hupert, A. D. Washburne, Using influenza surveillance networks to  
650 estimate state-specific prevalence of SARS-CoV-2 in the United States. *Science*  
651 *Translational Medicine* (2020), doi:10.1126/scitranslmed.abc1126.
- 652 7. D. Böhning, I. Rocchetti, A. Maruotti, H. Holling, Estimating the undetected infections in the  
653 Covid-19 outbreak by harnessing capture-recapture methods. *Int. J. Infect. Dis.* **97**, 197–201  
654 (2020).
- 655 8. Y. H. Baek, J. Um, K. J. C. Antigua, J.-H. Park, Y. Kim, S. Oh, Y. Kim, W.-S. Choi, S. G.  
656 Kim, J. H. Jeong, B. S. Chin, H. D. G. Nicolas, J.-Y. Ahn, K. S. Shin, Y. K. Choi, J.-S. Park,  
657 M.-S. Song, Development of a reverse transcription-loop-mediated isothermal amplification  
658 as a rapid early-detection method for novel SARS-CoV-2. *Emerg Microbes Infect.* **9**, 998–  
659 1007 (2020).
- 660 9. L. Leo, Mylab gets commercial approval from ICMR for Covid-19 antigen rapid testing kit.  
661 *Livemint* (2020), (available at [https://www.livemint.com/news/india/mylab-gets-commercial-](https://www.livemint.com/news/india/mylab-gets-commercial-approval-from-icmr-for-covid-19-antigen-rapid-testing-kit-11595434040321.html)  
662 [approval-from-icmr-for-covid-19-antigen-rapid-testing-kit-11595434040321.html](https://www.livemint.com/news/india/mylab-gets-commercial-approval-from-icmr-for-covid-19-antigen-rapid-testing-kit-11595434040321.html)).
- 663 10. S. Dey, Coronavirus testing: Rapid antigen tests now make up nearly half of daily checks |  
664 India News - Times of India. *The Times of India*, (available at  
665 [https://timesofindia.indiatimes.com/india/rapid-antigen-tests-now-make-up-nearly-half-of-](https://timesofindia.indiatimes.com/india/rapid-antigen-tests-now-make-up-nearly-half-of-daily-checks/articleshow/77340459.cms)  
666 [daily-checks/articleshow/77340459.cms](https://timesofindia.indiatimes.com/india/rapid-antigen-tests-now-make-up-nearly-half-of-daily-checks/articleshow/77340459.cms)).
- 667 11. C. B. F. Vogels, A. F. Brito, A. L. Wyllie, J. R. Fauver, I. M. Ott, C. C. Kalinich, M. E.  
668 Petrone, A. Casanovas-Massana, M. Catherine Muenker, A. J. Moore, J. Klein, P. Lu, A. Lu-  
669 Culligan, X. Jiang, D. J. Kim, E. Kudo, T. Mao, M. Moriyama, J. E. Oh, A. Park, J. Silva, E.

- 670 Song, T. Takahashi, M. Taura, M. Tokuyama, A. Venkataraman, O.-E. Weizman, P. Wong,  
671 Y. Yang, N. R. Cheemarla, E. B. White, S. Lapidus, R. Earnest, B. Geng, P. Vijayakumar, C.  
672 Odio, J. Fournier, S. Bermejo, S. Farhadian, C. S. Dela Cruz, A. Iwasaki, A. I. Ko, M. L.  
673 Landry, E. F. Foxman, N. D. Grubaugh, Analytical sensitivity and efficiency comparisons of  
674 SARS-CoV-2 RT-qPCR primer-probe sets. *Nat Microbiol* (2020), doi:10.1038/s41564-020-  
675 0761-6.
- 676 12. D. B. Larremore, B. Wilder, E. Lester, S. Shehata, J. M. Burke, J. A. Hay, M. Tambe, M. J.  
677 Mina, R. Parker, Test sensitivity is secondary to frequency and turnaround time for COVID-  
678 19 surveillance. *medRxiv* (2020), doi:10.1101/2020.06.22.20136309.
- 679 13. Z. Shen, F. Ning, W. Zhou, X. He, C. Lin, D. P. Chin, Z. Zhu, A. Schuchat, Superspreading  
680 SARS events, Beijing, 2003. *Emerging Infect. Dis.* **10**, 256–260 (2004).
- 681 14. J. S. M. Peiris, C. M. Chu, V. C. C. Cheng, K. S. Chan, I. F. N. Hung, L. L. M. Poon, K. I.  
682 Law, B. S. F. Tang, T. Y. W. Hon, C. S. Chan, K. H. Chan, J. S. C. Ng, B. J. Zheng, W. L.  
683 Ng, R. W. M. Lai, Y. Guan, K. Y. Yuen, HKU/UCH SARS Study Group, Clinical  
684 progression and viral load in a community outbreak of coronavirus-associated SARS  
685 pneumonia: a prospective study. *Lancet.* **361**, 1767–1772 (2003).
- 686 15. X. He, E. H. Y. Lau, P. Wu, X. Deng, J. Wang, X. Hao, Y. C. Lau, J. Y. Wong, Y. Guan, X.  
687 Tan, X. Mo, Y. Chen, B. Liao, W. Chen, F. Hu, Q. Zhang, M. Zhong, Y. Wu, L. Zhao, F.  
688 Zhang, B. J. Cowling, F. Li, G. M. Leung, Temporal dynamics in viral shedding and  
689 transmissibility of COVID-19. *Nat. Med.* **26**, 672–675 (2020).

- 690 16. J. Bullard, K. Dust, D. Funk, J. E. Strong, D. Alexander, L. Garnett, C. Boodman, A. Bello,  
691 A. Hedley, Z. Schiffman, K. Doan, N. Bastien, Y. Li, P. G. Van Caesele, G. Poliquin,  
692 Predicting infectious SARS-CoV-2 from diagnostic samples. *Clin. Infect. Dis.* (2020),  
693 doi:10.1093/cid/ciaa638.
- 694 17. G. Giordano, F. Blanchini, R. Bruno, P. Colaneri, A. Di Filippo, A. Di Matteo, M. Colaneri,  
695 Modelling the COVID-19 epidemic and implementation of population-wide interventions in  
696 Italy. *Nat. Med.* **26**, 855–860 (2020).
- 697 18. S. Choi, M. Ki, Estimating the reproductive number and the outbreak size of COVID-19 in  
698 Korea. *Epidemiol Health.* **42**, e2020011 (2020).
- 699 19. Y. Y. Wei, Z. Z. Lu, Z. C. Du, Z. J. Zhang, Y. Zhao, S. P. Shen, B. Wang, Y. T. Hao, F.  
700 Chen, [Fitting and forecasting the trend of COVID-19 by SEIR(+CAQ) dynamic model].  
701 *Zhonghua Liu Xing Bing Xue Za Zhi.* **41**, 470–475 (2020).
- 702 20. Z. Yang, Z. Zeng, K. Wang, S.-S. Wong, W. Liang, M. Zanin, P. Liu, X. Cao, Z. Gao, Z.  
703 Mai, J. Liang, X. Liu, S. Li, Y. Li, F. Ye, W. Guan, Y. Yang, F. Li, S. Luo, Y. Xie, B. Liu,  
704 Z. Wang, S. Zhang, Y. Wang, N. Zhong, J. He, Modified SEIR and AI prediction of the  
705 epidemics trend of COVID-19 in China under public health interventions. *J Thorac Dis.* **12**,  
706 165–174 (2020).
- 707 21. S. Cao, P. Feng, P. Shi, [Study on the epidemic development of COVID-19 in Hubei  
708 province by a modified SEIR model]. *Zhejiang Da Xue Xue Bao Yi Xue Ban.* **49**, 178–184  
709 (2020).



- 710 22. R. Huang, M. Liu, Y. Ding, Spatial-temporal distribution of COVID-19 in China and its  
711 prediction: A data-driven modeling analysis. *J Infect Dev Ctries.* **14**, 246–253 (2020).
- 712 23. A. Godio, F. Pace, A. Vergnano, SEIR Modeling of the Italian Epidemic of SARS-CoV-2  
713 Using Computational Swarm Intelligence. *Int J Environ Res Public Health.* **17** (2020),  
714 doi:10.3390/ijerph17103535.
- 715 24. M. Gatto, E. Bertuzzo, L. Mari, S. Miccoli, L. Carraro, R. Casagrandi, A. Rinaldo, Spread  
716 and dynamics of the COVID-19 epidemic in Italy: Effects of emergency containment  
717 measures. *Proc. Natl. Acad. Sci. U.S.A.* **117**, 10484–10491 (2020).
- 718 25. C. Hou, J. Chen, Y. Zhou, L. Hua, J. Yuan, S. He, Y. Guo, S. Zhang, Q. Jia, C. Zhao, J.  
719 Zhang, G. Xu, E. Jia, The effectiveness of quarantine of Wuhan city against the Corona  
720 Virus Disease 2019 (COVID-19): A well-mixed SEIR model analysis. *J. Med. Virol.* **92**,  
721 841–848 (2020).
- 722 26. T. Zhou, Q. Liu, Z. Yang, J. Liao, K. Yang, W. Bai, X. Lu, W. Zhang, Preliminary prediction  
723 of the basic reproduction number of the Wuhan novel coronavirus 2019-nCoV. *J Evid Based*  
724 *Med.* **13**, 3–7 (2020).
- 725 27. C. Reno, J. Lenzi, A. Navarra, E. Barelli, D. Gori, A. Lanza, R. Valentini, B. Tang, M. P.  
726 Fantini, Forecasting COVID-19-Associated Hospitalizations under Different Levels of  
727 Social Distancing in Lombardy and Emilia-Romagna, Northern Italy: Results from an  
728 Extended SEIR Compartmental Model. *J Clin Med.* **9** (2020), doi:10.3390/jcm9051492.

- 729 28. F. Yu, L. Yan, N. Wang, S. Yang, L. Wang, Y. Tang, G. Gao, S. Wang, C. Ma, R. Xie, F.  
730 Wang, C. Tan, L. Zhu, Y. Guo, F. Zhang, Quantitative Detection and Viral Load Analysis of  
731 SARS-CoV-2 in Infected Patients. *Clin. Infect. Dis.* **71**, 793–798 (2020).
- 732 29. S. N. Rao, D. Manissero, V. R. Steele, J. Pareja, A Narrative Systematic Review of the  
733 Clinical Utility of Cycle Threshold Values in the Context of COVID-19. *Infect Dis Ther*, 1–  
734 14 (2020).
- 735 30. J. Alizargar, Risk of reactivation or reinfection of novel coronavirus (COVID-19). *J.*  
736 *Formos. Med. Assoc.* **119**, 1123 (2020).
- 737 31. D. Batisse, N. Benech, E. Botelho-Nevers, K. Bouiller, R. Collarino, A. Conrad, L. Gallay,  
738 F. Goehringer, M. Gousseff, D. C. Joseph, A. Lemaigren, F.-X. Lescure, B. Levy, M.  
739 Mahevas, P. Penot, B. Pozzetto, D. Salmon, D. Slama, N. Vignier, B. Wyplosz, Clinical  
740 recurrences of COVID-19 symptoms after recovery: viral relapse, reinfection or  
741 inflammatory rebound? *J. Infect.* (2020), doi:10.1016/j.jinf.2020.06.073.
- 742 32. W. Deng, L. Bao, J. Liu, C. Xiao, J. Liu, J. Xue, Q. Lv, F. Qi, H. Gao, P. Yu, Y. Xu, Y. Qu,  
743 F. Li, Z. Xiang, H. Yu, S. Gong, M. Liu, G. Wang, S. Wang, Z. Song, Y. Liu, W. Zhao, Y.  
744 Han, L. Zhao, X. Liu, Q. Wei, C. Qin, Primary exposure to SARS-CoV-2 protects against  
745 reinfection in rhesus macaques. *Science* (2020), doi:10.1126/science.abc5343.
- 746 33. M. Ota, Will we see protection or reinfection in COVID-19? *Nat. Rev. Immunol.* **20**, 351  
747 (2020).

- 748 34. A. Victor Okhuese, Estimation of the Probability of Reinfection With COVID-19 by the  
749 Susceptible-Exposed-Infectious-Removed-Undetectable-Susceptible Model. *JMIR Public*  
750 *Health Surveill.* **6**, e19097 (2020).
- 751 35. Y. Gu, COVID-19 Projections Using Machine Learning. *COVID-19 Projections Using*  
752 *Machine Learning*, (available at <https://covid19-projections.com/>).
- 753 36. D. Stadlbauer, J. Tan, K. Jiang, M. Hernandez, S. Fabre, F. Amanat, C. Teo, G. A.  
754 Arunkumar, M. McMahon, J. Jhang, M. Nowak, V. Simon, E. Sordillo, H. van Bakel, F.  
755 Krammer, *medRxiv*, in press, doi:10.1101/2020.06.28.20142190.
- 756 37. A. Goodnough, M. D. Shear, The U.S.'s Slow Start to Coronavirus Testing: A Timeline. *The*  
757 *New York Times* (2020), (available at [https://www.nytimes.com/2020/03/28/us/coronavirus-](https://www.nytimes.com/2020/03/28/us/coronavirus-testing-timeline.html)  
758 [testing-timeline.html](https://www.nytimes.com/2020/03/28/us/coronavirus-testing-timeline.html)).
- 759 38. M. D. Shear, A. Goodnough, S. Kaplan, S. Fink, K. Thomas, N. Weiland, The Lost Month:  
760 How a Failure to Test Blinded the U.S. to Covid-19. *The New York Times* (2020), (available  
761 at <https://www.nytimes.com/2020/03/28/us/testing-coronavirus-pandemic.html>).
- 762 39. S. Kaplan, K. Thomas, Despite Promises, Testing Delays Leave Americans 'Flying Blind.'  
763 *The New York Times* (2020), (available at  
764 <https://www.nytimes.com/2020/04/06/health/coronavirus-testing-us.html>).
- 765 40. W. M. de Souza, L. F. Buss, D. da S. Candido, J.-P. Carrera, S. Li, A. E. Zarebski, R. H. M.  
766 Pereira, C. A. Prete, A. A. de Souza-Santos, K. V. Parag, M. C. T. D. Belotti, M. F.  
767 Vincenti-Gonzalez, J. Messina, F. C. da Silva Sales, P. dos S. Andrade, V. H. Nascimento, F.  
768 Ghilardi, L. Abade, B. Gutierrez, M. U. G. Kraemer, C. K. V. Braga, R. S. Aguiar, N.

- 769 Alexander, P. Mayaud, O. J. Brady, I. Marcilio, N. Gouveia, G. Li, A. Tami, S. B. de  
770 Oliveira, V. B. G. Porto, F. Ganem, W. A. F. de Almeida, F. F. S. T. Fantinato, E. M.  
771 Macário, W. K. de Oliveira, M. L. Nogueira, O. G. Pybus, C.-H. Wu, J. Croda, E. C. Sabino,  
772 N. R. Faria, Epidemiological and clinical characteristics of the COVID-19 epidemic in  
773 Brazil. *Nature Human Behaviour*. **4**, 856–865 (2020).
- 774 41. S. Mervosh, M. Fernandez, ‘It’s Like Having No Testing’: Coronavirus Test Results Are  
775 Still Delayed. *The New York Times* (2020), (available at  
776 <https://www.nytimes.com/2020/08/04/us/virus-testing-delays.html>).
- 777 42. K. Gostic, A. C. Gomez, R. O. Mummah, A. J. Kucharski, J. O. Lloyd-Smith, Estimated  
778 effectiveness of symptom and risk screening to prevent the spread of COVID-19. *eLife*. **9**,  
779 e55570 (2020).
- 780 43. T. Zitek, The Appropriate Use of Testing for COVID-19. *West J Emerg Med*. **21**, 470–472  
781 (2020).
- 782 44. I. Bosch, H. de Puig, M. Hiley, M. Carré-Camps, F. Perdomo-Celis, C. F. Narváez, D. M.  
783 Salgado, D. Senthoo, M. O’Grady, E. Phillips, A. Durbin, D. Fandos, H. Miyazaki, C.-W.  
784 Yen, M. Gélvez-Ramírez, R. V. Warke, L. S. Ribeiro, M. M. Teixeira, R. P. Almeida, J. E.  
785 Muñoz-Medina, J. E. Ludert, M. L. Nogueira, T. E. Colombo, A. C. B. Terzian, P. T. Bozza,  
786 A. S. Calheiros, Y. R. Vieira, G. Barbosa-Lima, A. Vizzoni, J. Cerbino-Neto, F. A. Bozza, T.  
787 M. L. Souza, M. R. O. Trugilho, A. M. B. de Filippis, P. C. de Sequeira, E. T. A. Marques,  
788 T. Magalhaes, F. J. Díaz, B. N. Restrepo, K. Marín, S. Mattar, D. Olson, E. J. Asturias, M.  
789 Lucera, M. Singla, G. R. Medigeshi, N. de Bosch, J. Tam, J. Gómez-Márquez, C. Clavet, L.

790 Villar, K. Hamad-Schifferli, L. Gehrke, Rapid antigen tests for dengue virus serotypes and  
791 Zika virus in patient serum. *Sci Transl Med.* **9** (2017), doi:10.1126/scitranslmed.aan1589.

792 45. Massachusetts Department of Public Health, COVID-19 Response Reporting. *Mass.gov*,  
793 (available at <https://www.mass.gov/info-details/covid-19-response-reporting>).

794 46. California Department of Public Health, COVID-19 Cases - California Open Data, (available  
795 at <https://data.ca.gov/dataset/covid-19-cases>).

796 47. California Department of Public Health, COVID-19 Hospital Data - California Open Data,  
797 (available at <https://data.ca.gov/dataset/covid-19-hospital-data>).

798 48. Department of Health and Human Hygiene, COVID-19 Daily Counts of Cases,  
799 Hospitalizations, and Deaths | NYC Open Data, (available at  
800 [https://data.cityofnewyork.us/Health/COVID-19-Daily-Counts-of-Cases-Hospitalizations-](https://data.cityofnewyork.us/Health/COVID-19-Daily-Counts-of-Cases-Hospitalizations-an/rc75-m7u3)  
801 [an/rc75-m7u3](https://data.cityofnewyork.us/Health/COVID-19-Daily-Counts-of-Cases-Hospitalizations-an/rc75-m7u3)).

802 49. Sao Jose do Rio Preto Public Health Office, “COVID-19 Surveillance Data, Sao Jose do Rio  
803 Preto” (Sao Jose do Rio Preto Public Health Office, Sao Jose do Rio Preto, Brazil).

804 50. New York State Government, Daily Hospitalization Summary by Region. *New York*  
805 *Forward*, (available at <https://forward.ny.gov/daily-hospitalization-summary-region>).

806 51. Massachusetts General Hospital Institute for Technology Assessment, COVID-19 Simulator  
807 - Methodology, (available at [https://www.covid19sim.org/images/docs/COVID-](https://www.covid19sim.org/images/docs/COVID-19_simulator_methodology_download_20200507.pdf)  
808 [19\\_simulator\\_methodology\\_download\\_20200507.pdf](https://www.covid19sim.org/images/docs/COVID-19_simulator_methodology_download_20200507.pdf)).

- 809 52. CDC, Coronavirus Disease 2019 (COVID-19). *Centers for Disease Control and Prevention*  
810 (2020), (available at <https://www.cdc.gov/coronavirus/2019-ncov/cases-updates/commercial->  
811 [lab-surveys.html](https://www.cdc.gov/coronavirus/2019-ncov/cases-updates/commercial-lab-surveys.html)).
- 812 53. SciPy.org — SciPy.org, (available at <https://www.scipy.org/>).
- 813 54. NumPy, (available at <https://numpy.org/>).
- 814 55. Non-Linear Least-Squares Minimization and Curve-Fitting for Python — Non-Linear Least-  
815 Squares Minimization and Curve-Fitting for Python, (available at  
816 <https://lmfit.github.io/lmfit-py/>).
- 817 56. Matplotlib: Python plotting — Matplotlib 3.3.1 documentation, (available at  
818 <https://matplotlib.org/>).
- 819 57. Plotly: The front-end for ML and data science models, (available at <https://plotly.com/>).

820

821

## 822 **Acknowledgments**

823 **General:** We thank Professor Lee Gehrke for critical reading of the manuscript.

824 **Funding:** EN is funded by Tufts University DISC Seed Grant. MLN is supported by a  
825 FAPESP grant (#2020/04836-0) and is a CNPq Research Fellow. AFV is supported by a  
826 FAPESP Fellow grant (#18/17647-0). GRFC is supported by a FAPESP Fellow grant  
827 (#20/07419-0). BHGAM is supported by a FAPESP Scholarship (#19/06572-2). The  
828 funders had no role in the design of the study; in the collection, analyses, or interpretation  
829 of data; in the writing of the manuscript, or in the decision to publish the results.

830 **Author contributions:** Conceptualization: BBH. Formal analysis: BN, AB, AR, MB,  
831 NS, ARG, AV, GCDS, TMILDS, BHGAM, MMM, GRFC, FQ, AFNR, MLG, ENN, IB,  
832 BBH. Funding acquisition: IB, BBH. Investigation: BN, AB, AR, MB, NS, ARG, AV,  
833 GCDS, TMILDS, BHGAM, MMM, GRFC, FQ, AFNR, MLG, ENN, IB, BBH.  
834 Methodology: BN, AB, AR, MB, NS, ARG, AV, GCDS, TMILDS, BHGAM, MMM,  
835 GRFC, FQ, AFNR, MLG, ENN, IB, BBH. Project administration: MLN, IB, BBH.  
836 Resources: MLN, IB, BBH. Supervision: MB, MLN, ENN, IB, BBH. Validation: BN,  
837 AB, AR, MB, ENN, BBH. Visualization: BN, AB, AR, MB, AV, ENN, BBH. Writing—  
838 original draft: AR, BBH. Writing—review and editing: BN, AB, AR, MB, NS, ARG,  
839 AV, GCDS, TMILDS, BHGAM, MMM, GRFC, FQ, AFNR, MLG, ENN, IB, BBH.  
840 **Competing interests:** BN, AB, AR, MB, NS, AG, IB, and BBH are employed by or  
841 affiliated with E25Bio Inc. ([www.e25bio.com](http://www.e25bio.com)), a company that develops diagnostics for  
842 epidemic viruses.

843

844

## 845 **Figures and Tables**

846

## 847 **TABLES**

848

849 **Table 1. Clinical validation summary for the direct antigen rapid test (DART) for SARS-**  
850 **CoV-2 nucleocapsid protein evaluated using 190 retrospectively collected patient nasal**  
851 **swab specimens.**

852

All Data Summary								
		qRT-PCR (gene average)					95% Confidence Interval	
		+	-	Total	Sensitivity	80.0%	76.1%	83.9%
DART (nucleocapsid protein)	+	80	8	88	Specificity	91.1%	88.2%	94.0%
	-	20	82	102	Positive Predictive Value	90.9%	87.9%	93.9%
Total		100	90	190	Negative Predictive Value	80.4%	76.6%	84.2%
					Prevalence	52.6%	47.8%	57.5%
					Overall Agreement	85.3%	82.8%	87.8%

853

854

855

856

857

858

859

860

861 **Table 2. Clinical validation summary for the SARS-CoV-2 direct antigen rapid test**

862 **(DART) for SARS-SoC-2 spike glycoprotein evaluated using 121 retrospectively collected**

863 **patient nasopharyngeal swab specimens.**

864

865



All Data Summary								
		qRT-PCR (gene average)					95% Confidence Interval	
		+	-	Total	Sensitivity	84.7%	80.6%	88.9%
DART (spike glycoprotein)	+	61	7	68	Specificity	85.7%	80.8%	90.6%
	-	11	42	53	Positive Predictive Value	89.7%	86.2%	93.2%
Total		72	49	121	Negative Predictive Value	79.2%	73.6%	84.9%
					Prevalence	59.5%	53.9%	65.1%
					Overall Agreement	85.1%	82.0%	88.3%

866

867

868

869

870

871

872

873

874

875

876

877 **Table 3. Details of parameter values used for *SIDHRE-Q* Model.**

878

Parameter	Details & Statistics			
	$\alpha$ is the probability that an interaction between an undetected infected person and		Mean	St. Dev.

$\alpha$	an uninfected person results in a new infection, divided by the average number of uninfected people an undetected infected person comes into contact with on a given day. $\alpha$ is estimated from the data.	MA	0.088	0.051
		LA	0.090	0.034
		NYC	0.067	0.042
		SJRP	0.121	0.042
$\eta$	<p><math>\eta</math> is the probability that an interaction between an infected person and an uninfected person results in a new infection, divided by the average number of uninfected people a detected infected person comes into contact with on a given day. <math>\eta = 0.01 \cdot \alpha</math></p> <p>The constant relating <math>\eta, \alpha</math> accounts for a small but nonzero transmission due to the quarantined (detected) infected population. This value was chosen to be small, assuming a quarantined individual will only infect others with low probability.</p>			
$\nu$	$\nu$ is the probability that a symptomatic undetected individual is diagnosed on a given day. $\nu$ is estimated from the data. $\nu$ is multiplied by sensitivity (assume benchmark sensitivity 100% for PCR, as used when fitting).		Mean	St. Dev.
		MA	0.006	0.005
		LA	0.011	0.006
		NYC	0.0056	0.002
		SJRP	0.015	0.007
$\epsilon$	$\epsilon$ is the probability that an asymptomatic undetected infected individual is diagnosed on a given day. $\epsilon = 0$ while fitting (during PCR symptomatic testing). $\epsilon = (\text{sensitivity}/\text{days between tests})$ when the rapid testing strategy is activated.			
$\lambda$	$\lambda$ is the probability that an undetected infected individual transitions to the recovered state on a given day. $\lambda = 1/14$ , or the inverse of average recovery time ( $5I$ ).			
$\mu$	$\mu$ is the probability that an infected individual develops severe symptoms on a given day and transitions into the hospitalized state. The flow from $D$ to $H$ is assumed to be independent of the ratio $I/D$ , but comes only from the detected infected population, hence why it is multiplied by $(I + D)/D$ . $\mu$ is estimated from the data.		Mean	St. Dev.
		MA	0.0013	9.5e-4
		LA	0.0016	2.4e-4
		NYC	0.0011	6.6e-4
		SJRP	0.0018	8.0e-4
$\rho$	<p><math>\rho</math> is the probability that a detected infected individual transitions to the recovered state on a given day.</p> <p><math>\rho = 1/14</math>, or the inverse of the average recovery time (<math>5I</math>).</p>			
$\sigma$	$\sigma$ is the probability that a hospitalized individual transitions to the recovered state on a given day. $\sigma = 1/11$ , or the inverse of the average recovery time for a hospitalized individual ( $5I$ ).			
$\tau$	$\tau$ is the probability that a hospitalized individual expires on a given day. $\tau$ is estimated from the data.		Mean	St. Dev.
		MA	0.034	0.012

		LA	0.016	0.004
		NYC	0.036	0.034
		SJRP	0.032	0.045
$\gamma$	$\gamma$ is the probability of entering either of the quarantine states on a given day from either the Susceptible or Recovered populations. $\gamma = 0$ while fitting (during PCR symptomatic testing). $\gamma = (1 - \text{specificity}) \times (1/\text{days between tests})$ when the rapid testing strategy is activated.			
$\psi$	$\psi$ is the probability that an individual exits quarantine on a given day. $\psi = 1/14$ , or the inverse of the quarantine period for fixed length quarantine.			
Parameter	Details & Statistics			
$\alpha$	$\alpha$ is the probability that an interaction between an undetected infected person and an uninfected person results in a new infection, divided by the average number of uninfected people an undetected infected person comes into contact with on a given day. $\alpha$ is estimated from the data.		Mean	St. Dev.
		MA	0.088	0.051
		LA	0.090	0.034
		NYC	0.067	0.042
		SJRP	0.121	0.042
$\eta$	$\eta$ is the probability that an interaction between an infected person and an uninfected person results in a new infection, divided by the average number of uninfected people a detected infected person comes into contact with on a given day. $\eta = 0.01 \cdot \alpha$ The constant relating $\eta, \alpha$ accounts for a small but nonzero transmission due to the quarantined (detected) infected population. This value was chosen to be small, assuming a quarantined individual will only infect others with low probability.			
$\nu$	$\nu$ is the probability that a symptomatic undetected individual is diagnosed on a given day. $\nu$ is estimated from the data. $\nu$ is multiplied by sensitivity (assume benchmark sensitivity 100% for PCR, as used when fitting).		Mean	St. Dev.
		MA	0.006	0.005
		LA	0.011	0.006
		NYC	0.0056	0.002
SJRP			0.015	0.007
$\epsilon$	$\epsilon$ is the probability that an asymptomatic undetected infected individual is diagnosed on a given day. $\epsilon = 0$ while fitting (during PCR symptomatic testing). $\epsilon = (\text{sensitivity}/\text{days between tests})$ when the rapid testing strategy is activated.			
$\lambda$	$\lambda$ is the probability that an undetected infected individual transitions to the recovered state on a given day. $\lambda = 1/14$ , or the inverse of average recovery time ( $5I$ ).			
$\mu$	$\mu$ is the probability that an infected individual develops severe symptoms on a		Mean	St. Dev.

	given day and transitions into the hospitalized state. The flow from $\overline{D}$ to $\overline{H}$ is assumed to be independent of the ratio $\overline{I}/\overline{D}$ , but comes only from the detected infected population, hence why it is multiplied by $\overline{(I+D)}/\overline{D}$ . $\overline{\mu}$ is estimated from the data.	MA	0.0013	9.5e-4
		LA	0.0016	2.4e-4
		NYC	0.0011	6.6e-4
		SJRP	0.0018	8.0e-4
$\overline{\rho}$	$\overline{\rho}$ is the probability that a detected infected individual transitions to the recovered state on a given day. $\overline{\rho} = 1/14$ , or the inverse of the average recovery time (51).			
$\overline{\sigma}$	$\overline{\sigma}$ is the probability that a hospitalized individual transitions to the recovered state on a given day. $\overline{\sigma} = 1/11$ , or the inverse of the average recovery time for a hospitalized individual (51).			
$\overline{\tau}$	$\overline{\tau}$ is the probability that a hospitalized individual expires on a given day. $\overline{\tau}$ is estimated from the data.		Mean	St. Dev.
		MA	0.034	0.012
		LA	0.016	0.004
		NYC	0.036	0.034
		SJRP	0.032	0.045
$\overline{\gamma}$	$\overline{\gamma}$ is the probability of entering either of the quarantine states on a given day from either the Susceptible or Recovered populations. $\overline{\gamma} = 0$ while fitting (during PCR symptomatic testing). $\overline{\gamma} = (1 - \text{specificity}) \times (1/$ days between tests $)$ when the rapid testing strategy is activated.			
$\overline{\psi}$	$\overline{\psi}$ is the probability that an individual exits quarantine on a given day. $\overline{\psi} = 1/14$ , or the inverse of the quarantine period for fixed length quarantine.			

879

880

881

882

883 **FIGURES**

884

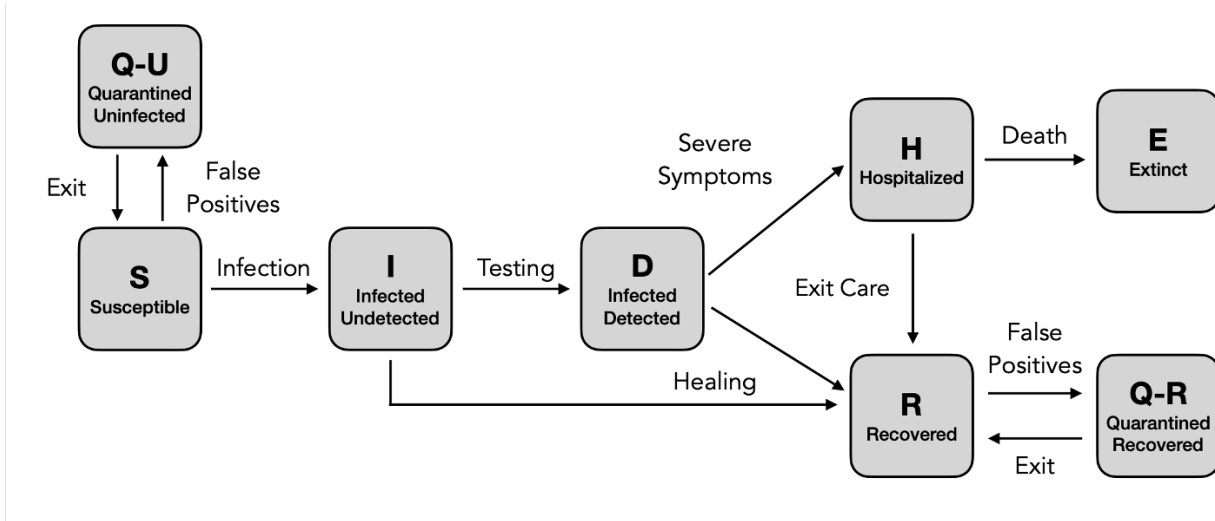
885 **Figure 1. Graphical scheme displaying the relationships between the stages of quarantine**

886 **and infection in *SIDHRE-Q* model. Q-U, quarantine uninfected; S, susceptible (uninfected); I,**

887 **infected undetected (pre-testing and infected); D, infected detected (infection diagnosis through**

888 testing); **H**, hospitalized (infected with life threatening symptom progression); **R**, recovered  
 889 (healed); **E**, extinct (dead); and **Q-R**, quarantine recovered (healed but in quarantine by false  
 890 positive testing).

891



892

893

894

895

896

897

898

899

900 **Figure 2. COVID-19 Outcomes in 3 US Regions and Brazil as a result of Frequent Rapid**

901 **Testing Protocol using the *SIDHRE-Q* Model. (A) The Cumulative Detected Infected,**

902 **Hospitalized, Deceased, Active Infections, Recovered, and Quarantined are modeled over 105**

903 **days (top to bottom) using reported data from 4 global regions: Massachusetts, Los Angeles,**

904 **New York City, and São José do Rio Preto in Brazil (left to right). The COVID-19 population**

905 spread and outcomes are modeled under a Rapid Testing Protocol (sensitivity 80%, specificity  
906 90%) with variable testing frequencies ranging from 1-21 days between tests. This protocol is  
907 compared to a symptom-based Rapid Testing protocol and a symptom-based PCR protocol. (B)  
908 Effect of Rapid Testing Protocol under variable testing sensitivities (30%-90%) and increasing  
909 frequency under the *SIDHRE-Q* Model. The Cumulative Infections, Maximum Simultaneously  
910 Hospitalized, and Deceased populations are modeled for Massachusetts, Los Angeles, New York  
911 City, and São José do Rio Preto in Brazil with a 90% test specificity.

912

913

914

915

916

917

918

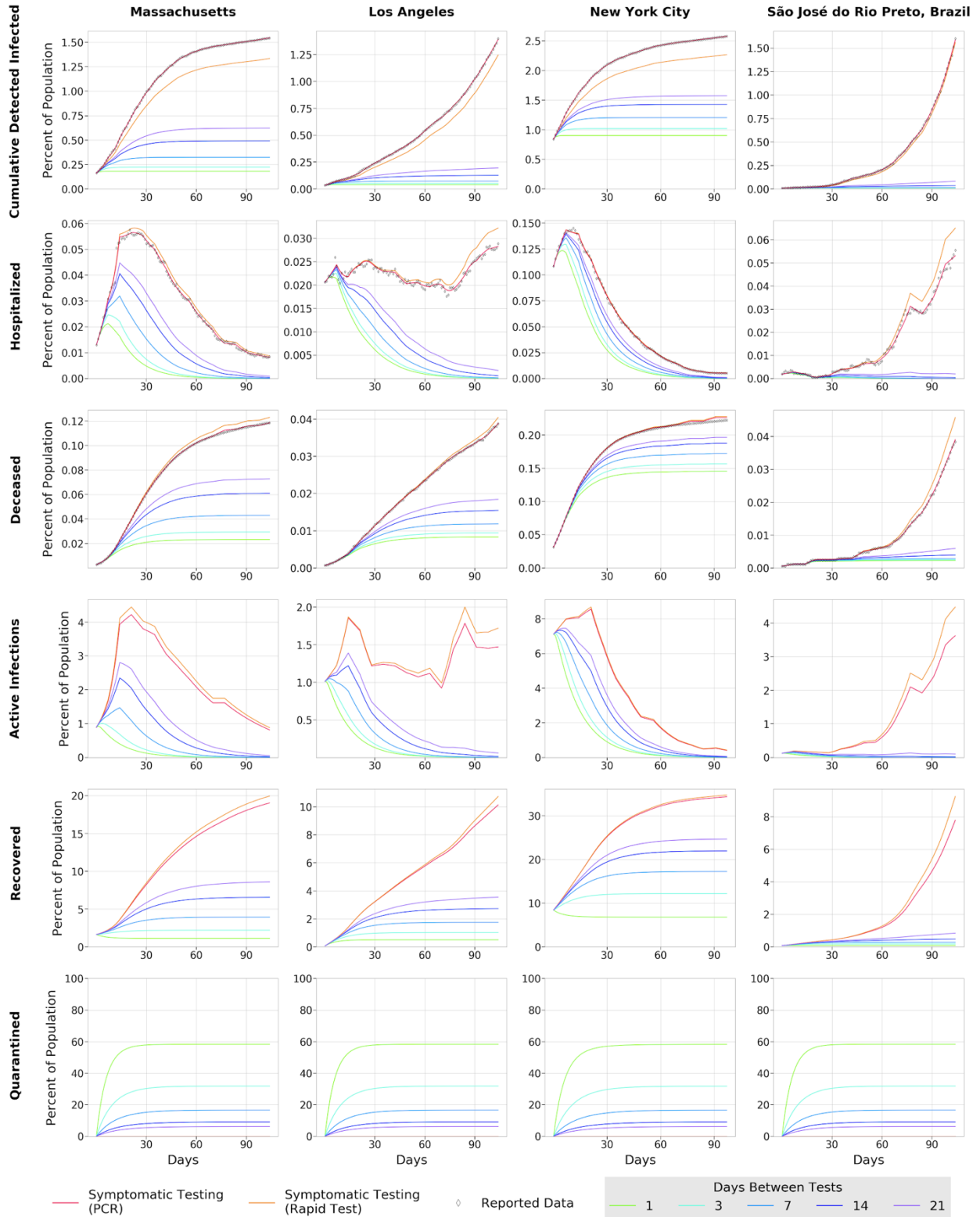
919

920

921

922

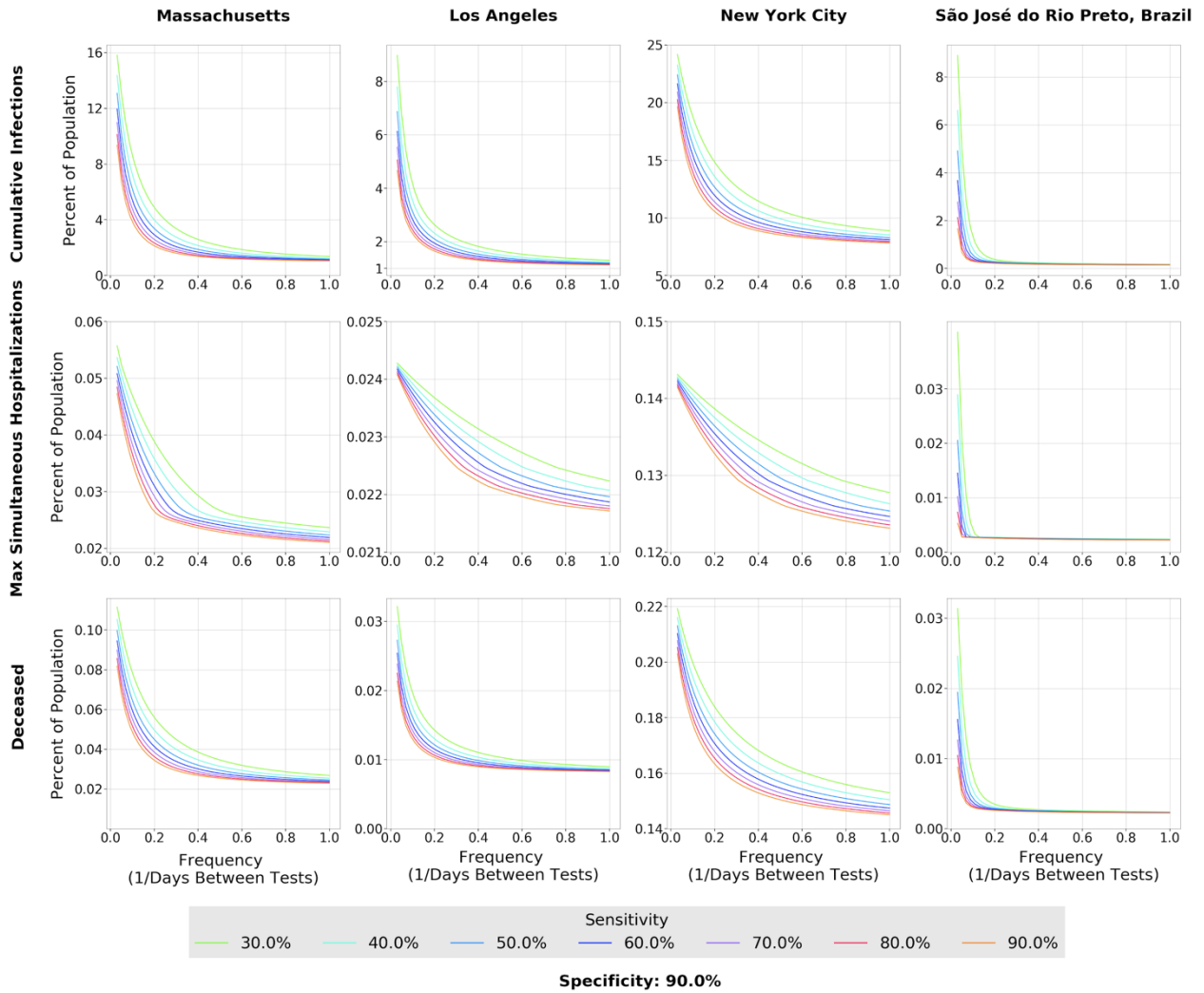
923 (A)



Sensitivity: 80.0% Specificity: 90.0%

924  
925

(B)



926

927

928

929

930

931

932

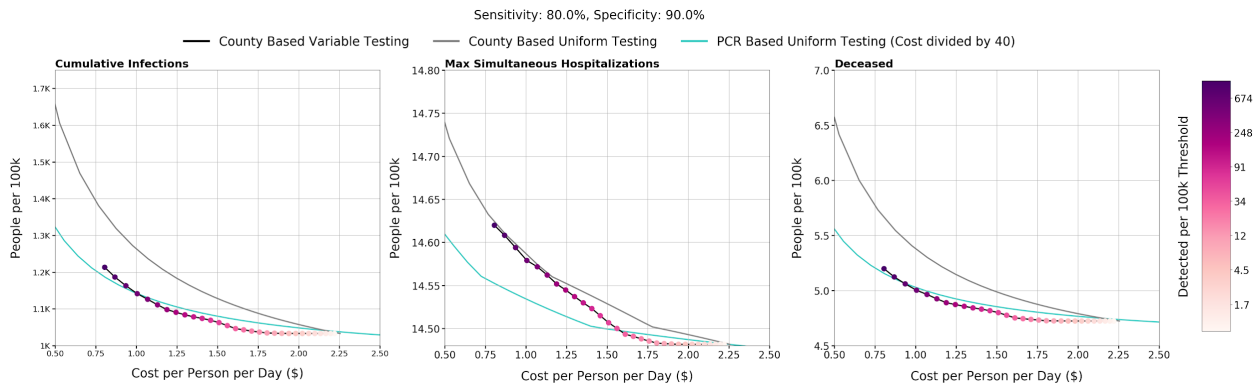
933

934



935 **Figure 3. Effect of County Based Rapid Testing strategy on COVID-19 outcomes in**  
 936 **California.** This protocol varies testing frequency in accordance to the number of recorded  
 937 cases; the threshold for number of active infections which, if reached, signals to commence  
 938 everyday testing (the highest frequency considered). A Rapid Test with a 80% sensitivity and  
 939 90% sensitivity versus is used in this deployment strategy. Shown is the total cost per person per  
 940 day versus the cumulative infections, maximum simultaneously hospitalized, and cumulative  
 941 deaths with varied thresholds for all of CA is shown. The County Based Rapid Testing strategy  
 942 is compared to uniform testing, which distributes the same number of total tests used in the  
 943 county strategy, albeit evenly across each county. The effects of uniform testing are modeled for  
 944 both a Rapid Testing protocol and a qRT-PCR protocol (A). The effects of County Based Rapid  
 945 Test Protocol and Uniform PCR Protocol on active infected detected population over time in CA  
 946 are shown (B). The legend denotes the thresholds at which testing frequency is determined, the  
 947 testing frequencies, the percent of CA population under the strategy, and the cost per person per  
 948 day.

951 (A)



952

953

